

CrossMark
click for updates

Cite this: DOI: 10.1039/c5ta01198a

Received 13th February 2015
Accepted 13th March 2015

DOI: 10.1039/c5ta01198a

www.rsc.org/MaterialsA

Nonvolatile chlorinated additives adversely influence $\text{CH}_3\text{NH}_3\text{PbI}_3$ based planar solar cells†

Yani Chen,^a Yixin Zhao^b and Ziqi Liang^{*a}

We demonstrate that nonvolatile CaCl_2 additives can significantly improve the film morphology of $\text{CH}_3\text{NH}_3\text{PbI}_3$. Unlike those volatile chlorinated additives, a small portion of Cl anions from CaCl_2 seem to enter into the $\text{CH}_3\text{NH}_3\text{PbI}_3$ crystal, yet most insulating CaCl_2 remains within the perovskite film, which is detrimental to perovskite solar cells.

Hybrid organic–inorganic halide perovskites have attracted significant attention owing to their extraordinary characteristics such as high absorption coefficient,¹ tunable optical bandgaps,² high carrier mobilities,³ and long electron and hole diffusion lengths.^{4,5} Within a very short timeframe, the power conversion efficiency (PCE) of perovskite based solar cells has rocketed to a certified 20.1%⁶ since they were first introduced.^{7–12}

Currently, most of the significant device enhancements have been achieved by the realization of high-quality perovskite films, suggesting that the film morphology such as uniformity and surface coverage is of prime importance for the high-efficiency operation of perovskite solar cells.^{13–16} The use of additives has been reported as a simple yet effective way of controlling the film morphology by successfully manipulating the nucleation and growth of the perovskite crystals, thereby improving the device performance. For instance, by adding HI, 1,8-diiodooctane (DIO) or $\text{CH}_3\text{NH}_3\text{Cl}$ to their corresponding standard precursor solutions, the continuous and uniform $\text{HC}(\text{NH}_2)_2\text{PbI}_3$, $\text{CH}_3\text{NH}_3\text{PbI}_{3-x}\text{Cl}_x$ or $\text{CH}_3\text{NH}_3\text{PbI}_3$ films were made, respectively.^{17–20} Most of these reported additives are then evaporated or sublimed during the thermal annealing step.

Moreover, recent studies showed that Cl^- had a great impact on the crystallization dynamics.^{18,20–23} The Cl incorporation has

proved to yield a longer diffusion length of carriers ($\sim 1 \mu\text{m}$)⁵ and higher electrical conductivity.²⁴ However, the function of chloride ions in the formation of perovskite film remains a mystery.

Herein, we prepare a dense and uniform perovskite film by adding nonvolatile compounds such as NaCl and CaCl_2 additives to the standard $\text{CH}_3\text{NH}_3\text{PbI}_3$ precursor solution consisting of an equimolar mixture of $\text{CH}_3\text{NH}_3\text{I}$ and PbI_2 . It was found that Cl^- had a significant influence on the film morphology by altering the kinetics of perovskite crystal growth. Interestingly, XRD measurements verify the formation of an intermediate phase preceding the crystallization, which helps to avoid incomplete and uneven surface coverage. Unlike those volatile additives such as $\text{CH}_3\text{NH}_3\text{Cl}$ and HI, most of the added insulating CaCl_2 remains in the final perovskite film, which is detrimental to the device performance, despite the partial inclusion into the $\text{CH}_3\text{NH}_3\text{PbI}_3$ crystal. We therefore argue that good additives used in solution chemistry of the perovskite film should not only enable to improve the film morphology but also possess the removability. Note that other inorganic chloride salts such as NaCl have similar effects on such film formation. We choose CaCl_2 as a proof-of-concept due to its relatively large solubility in DMF compared to NaCl.

All perovskite films were prepared *via* the one-step solution method on the quartz substrate from $\text{CH}_3\text{NH}_3\text{I} : \text{PbI}_2 : \text{CaCl}_2$ precursor mixtures with a molar ratio of 1 : 1 : 0.5, followed by thermal annealing at 95 °C. Fig. 1 compares optical spectra of annealed perovskite films over annealing time with the starting film before annealing. The unannealed perovskite film exhibits a typical absorption spectrum of $\text{CH}_3\text{NH}_3\text{PbI}_3$.²⁵ With an increase in thermal annealing time, the annealed perovskite film shows an increase in the visible absorbance across the entire spectral range, particularly in the range of 600–750 nm, and remains unchanged after 20 min, indicating that the conversion of the perovskite crystal structure is complete.

Scanning electron microscopy (SEM) was conducted to explore the effect of CaCl_2 in precursor solution on the

^aDepartment of Materials Science, Fudan University, Shanghai 200433, China. E-mail: zqliang@fudan.edu.cn

^bCollege of Environmental Science and Engineering, Shanghai Jiao Tong University, Shanghai 200240, China

† Electronic supplementary information (ESI) available: Experimental section and Table S1. See DOI: 10.1039/c5ta01198a

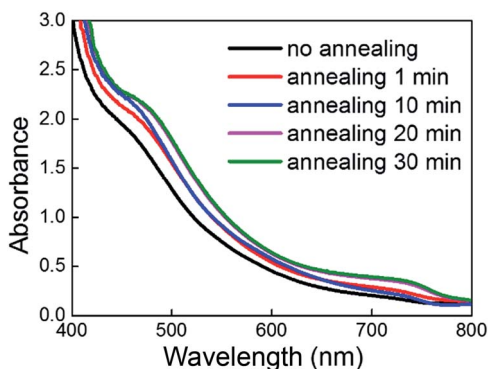


Fig. 1 Absorption spectra of the perovskite film obtained from $\text{CH}_3\text{NH}_3\text{I} : \text{PbI}_2 : \text{CaCl}_2$ precursor mixtures with 1 : 1 : 0.5 molar ratio with different thermal annealing times at 95 °C.

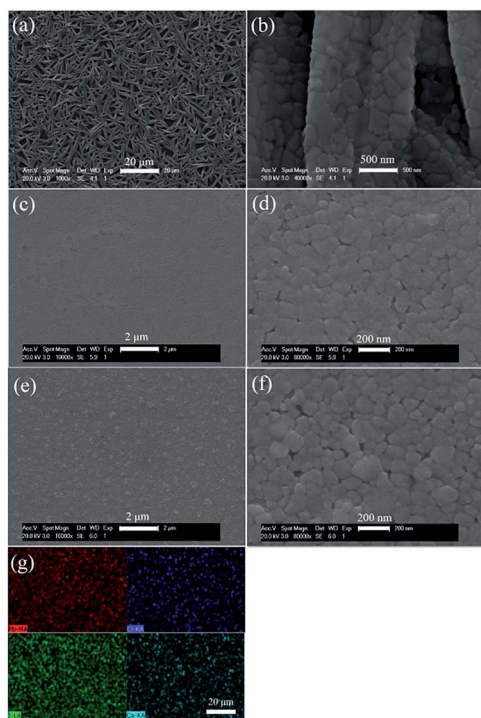


Fig. 2 SEM images of (a and b) the perovskite film prepared from standard precursor solution of $\text{CH}_3\text{NH}_3\text{I}$ and PbI_2 , (c and d) unannealed and (e and f) annealed perovskite films at 95 °C for 20 min obtained from $\text{CH}_3\text{NH}_3\text{I} : \text{PbI}_2 : \text{CaCl}_2$ precursor mixtures with 1 : 1 : 0.5 molar ratio. (g) EDX analysis of the annealed perovskite film: Pb map (red), I map (green), Ca map (light blue) and Cl map (dark blue).

perovskite film morphology. By using the standard precursor solution of $\text{CH}_3\text{NH}_3\text{I}$ and PbI_2 , as displayed in Fig. 2a and b, a poor film morphology is formed showing needle-shaped crystals and incomplete, uneven surface coverage, which is consistent with previous reports.^{20,26} By the addition of CaCl_2 , closely packed crystals are generated and the film becomes uniform with noticeably improved surface coverage as shown in Fig. 2c and d. This morphological variation caused by CaCl_2 is similar to the case of $\text{CH}_3\text{NH}_3\text{Cl}$.²⁰ It seems reasonable that free Cl^-

ionized from CaCl_2 in DMF solution plays a vital role in regulating the crystallization dynamics to improve the film topography. After thermal annealing for 20 min, some white spots show up. These tiny spots are probably the segregation of CaCl_2 , which could be attributed to thermally induced recrystallization of CaCl_2 (Fig. 2e and f). In addition, energy dispersive X-ray spectroscopy (EDX) mapping of a fully annealed perovskite film (Fig. 2d and e) discloses a homogeneous distribution of Pb, I, Ca and Cl elements throughout the whole film.

In order to further understand how Cl^- functions during the formation of the perovskite film, X-ray diffraction (XRD) measurements were carried out. Fig. 3a displays the XRD patterns of perovskite films obtained from $\text{CH}_3\text{NH}_3\text{I} : \text{PbI}_2 : \text{CaCl}_2$ precursor mixtures as a function of thermal annealing time, in comparison with the spin-coated CaCl_2 film. CaCl_2 exhibits an intense peak at 31.70°, while all perovskite films show strong diffraction peaks at 14.08°, 28.41° and 31.73°, assigned to the 110, 220, and 310 reflections of the tetragonal $\text{CH}_3\text{NH}_3\text{PbI}_3$ phase, respectively, which are in good agreement with other reports.^{27,28} Upon heat treatment, all these annealed perovskite films present similar XRD patterns in which all diffraction peaks become sharper and enhanced in intensity with increasing thermal annealing time due to improved crystallinity. It is worth noting that an additional peak of 10.70° appears in the unannealed perovskite film (Fig. 3b), which disappears after thermal annealing of only 1 min. This could be indicative of the formation of an instable intermediate phase induced by Cl^- preceding the crystallization step. A possible explanation is that this intermediate phase inhibits the formation of elongated crystals and incomplete coverage, and upon heat treatment it undergoes the rearrangement by releasing Cl^- , which is consistent with the SEM observation in Fig. 2. Moreover, the (310) diffraction peak at 31.73° of the CaCl_2 treated perovskite film that is overlapped with the characteristic peak of CaCl_2 at 31.70° is down-shifted and broadened with prolonged thermal annealing time. This is presumed to relate to the CaCl_2 recrystallization.

Furthermore, both EDX and X-ray photoelectron spectroscopy (XPS) results confirm the above assumption. The lead,

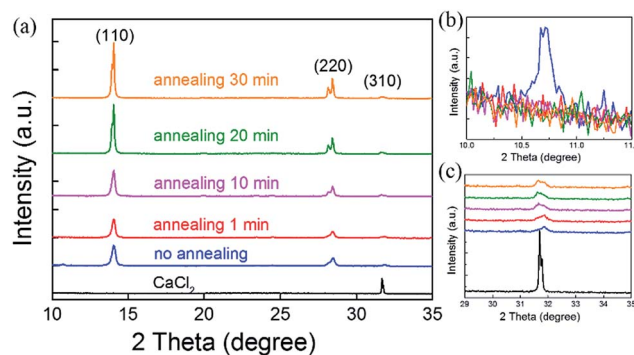


Fig. 3 (a) XRD patterns of CaCl_2 and perovskite films obtained from $\text{CH}_3\text{NH}_3\text{I} : \text{PbI}_2 : \text{CaCl}_2$ precursor mixtures showing the effects of thermal annealing time at 95 °C, respectively. Magnified XRD images of graph (a) ranging from (b) 10–11.5° and (c) 29–35°.

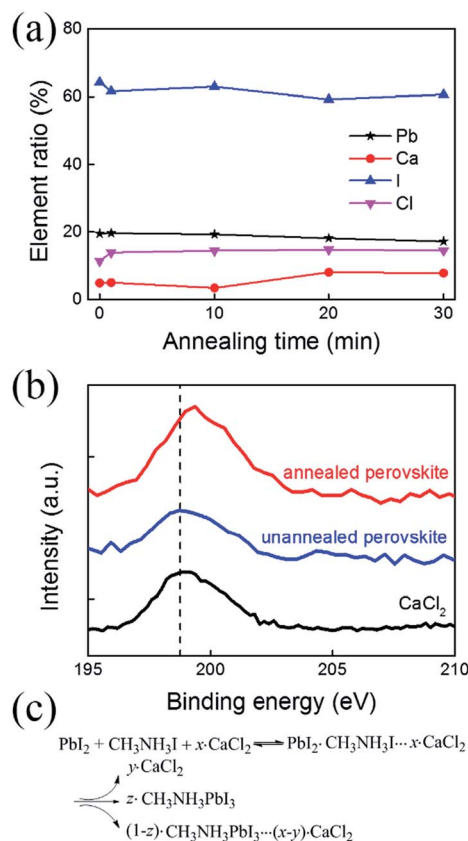


Fig. 4 (a) Atomic percentages of the main elements (Pb, Ca, I and Cl) revealed by EDX profiles in the perovskite films as a function of thermal annealing time. (b) XPS spectra (Cl 2p core level) of CaCl₂, unannealed and annealed perovskite films. (c) Possible chemical pathways among CaCl₂, CH₃NH₃I and PbI₂ during the formation of the perovskite film.

calcium, chlorine and iodine elements are detected in the perovskite films from the EDX profiles (Fig. 4a). The lead amount shows a slight drop while the amounts of chlorine and calcium exhibit a little increase as thermal annealing went on. This indicates that the low-density CaCl₂ agent may have migrated to the upper portion of the perovskite film, which coincides with SEM and XRD results of the recrystallization process of CaCl₂. To explore further where and how Cl is located and bonded in the perovskite film, XPS spectra were acquired as shown in Fig. 4b. The unannealed perovskite film has a 2p_{3/2} signal of Cl at 198.8 eV, the same as CaCl₂, suggesting the significant absence of Cl in the CH₃NH₃PbI₃ crystals. Note that the Cl signal in the annealed perovskite film has an up-shift by 0.5 eV, implying the likelihood of a partial inclusion of Cl into the CH₃NH₃PbI₃ crystals. Likely, most Cl⁻ ions precipitate out as CaCl₂ in the film after inducing a preferred orientation of CH₃NH₃PbI₃ crystal grains. In short, the possible chemical pathways among CaCl₂, CH₃NH₃I and PbI₂ during film formation are shown in Fig. 4c. The mixture of CaCl₂, CH₃NH₃I and PbI₂ first forms a kind of “solid solution”, which is unstable yet helpful in avoiding the formation of large needle-shaped CH₃NH₃PbI₃ crystals, resulting in the incomplete surface coverage. Then after heat treatment,

CH₃NH₃PbI₃ is successfully generated out of the solid solution, and most of the Cl⁻ and Ca²⁺ precipitate out in the form of CaCl₂ while Cl⁻ is partially incorporated into CH₃NH₃PbI₃ crystals. However, the exact chemical pathways are very difficult to determine due to the high instability of the intermediate state.

Finally, in order to test the effect of nonvolatile CaCl₂ on the photovoltaic performance of perovskite solar cells based on CH₃NH₃I : PbI₂ : CaCl₂ precursor mixtures with varied molar ratios, the solar cells were constructed with a typical configuration of the ITO/PEDOT:PSS/perovskite/PC₆₁BM/Ca/Al device with an active area of 0.11 cm². Fig. 5a–c show the photocurrent density versus voltage (*J*–*V*) curves of the best-performing CaCl₂ treated perovskite planar photovoltaic cells under AM 1.5G simulated light with an intensity of 100 mW cm⁻². The best cells' characteristics are summarized in Table S1† and their average values with a standard deviation of 10 individual devices are presented in Table S2.†

With the increasing molar ratio of CaCl₂, the device performs worse. Interestingly, the deterioration of device performance mainly lies in the short-circuit current density (*J*_{sc}) rather than the open-circuit voltage (*V*_{oc}). This agrees well with our other results, suggesting that the perovskite layer contains a certain amount of insulating CaCl₂. Note that the exact impact of the remaining Ca element remains unclear and needs further investigation. In addition, all of these devices exhibit the serious hysteresis. This could be explained by the fact that the perovskite layer here accumulates the charge carriers if the charges are not quickly transferred or transported into electron and hole conductors, respectively.^{29,30} Fig. 5d shows the representative external quantum efficiency (EQE) spectra of CaCl₂ treated perovskite cells, also showing a decrease of EQE with increasing proportion of CaCl₂, which indicates the aggravated photon-to-electron conversion.

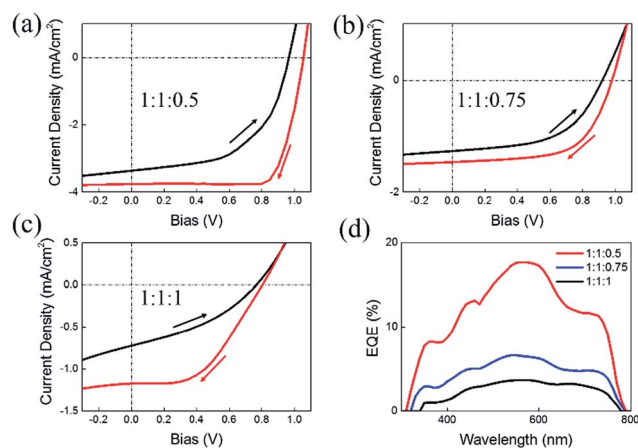


Fig. 5 Photocurrent density–voltage characteristics of regular ITO/PEDOT:PSS/perovskite/PC₆₁BM/Ca/Al solar cells measured under light at an intensity of 100 mW cm⁻² at forward (black line) and reverse (red line) scans, respectively, prepared from CH₃NH₃I : PbI₂ : CaCl₂ precursor mixtures with (a) 1 : 1 : 0.5, (b) 1 : 1 : 0.75, and (c) 1 : 1 : 1 molar ratio and (d) EQE spectrum of representative perovskite solar cells.

Conclusions

In summary, we have successfully prepared a uniform $\text{CH}_3\text{NH}_3\text{PbI}_3$ perovskite film with full surface coverage by adding the nonvolatile CaCl_2 additive into its precursor solution. CaCl_2 was found to modulate the crystallization kinetics and improve the film formation of perovskite. XRD measurements verify that an intermediate phase induced by Cl^- inclusion exists during the crystallization process. Moreover, EDX and XPS spectra show that upon heat treatment, most Cl^- ions precipitate out as insulating CaCl_2 from this intermediate phase and remain in the final perovskite film while a small amount of Cl^- ions may enter into the $\text{CH}_3\text{NH}_3\text{PbI}_3$ crystal. As a result, CaCl_2 treated $\text{CH}_3\text{NH}_3\text{PbI}_3$ based planar solar cells were shown to yield poor device performance.

Acknowledgements

This work was supported by the National Natural Science Foundation of China (NSFC) under grant no. 51473036 (Z. L.) and 51372151 (Y. Z.).

Notes and references

- H.-S. Kim, C.-R. Lee, J.-H. Im, K.-B. Lee, T. Moehl, A. Marchioro, S.-J. Moon, R. Humphry-Baker, J.-H. Yum, J. E. Moser, M. Grätzel and N.-G. Park, *Sci. Rep.*, 2012, **2**, 591.
- J. H. Noh, S. H. Im, J. H. Heo, T. N. Mandal and S. I. Seok, *Nano Lett.*, 2013, **13**, 1764.
- C. Wehrenfennig, G. E. Eperon, M. B. Johnston, H. J. Snaith and L. M. Herz, *Adv. Mater.*, 2014, **26**, 1584.
- S. D. Stranks, G. E. Eperon, G. Grancini, C. Menelaou, M. J. P. Alcocer, T. Leijtens, L. M. Herz, A. Petrozza and H. J. Snaith, *Science*, 2013, **342**, 341.
- G. Xing, N. Mathews, S. Sun, S. S. Lim, Y. M. Lam, M. Grätzel, S. Mhaisalkar and T. C. Sum, *Science*, 2013, **342**, 344.
- http://www.nrel.gov/ncpv/images/efficiency_chart.jpg, updated on Dec 18, 2014.
- A. Kojima, K. Teshima, Y. Shirai and T. Miyasaka, *J. Am. Chem. Soc.*, 2009, **131**, 6050.
- N. J. Jeon, J. H. Noh, W. S. Yang, Y. C. Kim, S. Ryu, J. Seo and S. I. Seok, *Nature*, 2015, **517**, 476.
- J. Burschka, N. Pellet, S. J. Moon, R. Humphry-Baker, P. Gao, M. K. Nazeeruddin and M. Grätzel, *Nature*, 2013, **499**, 316.
- M. M. Lee, J. Teuscher, T. Miyasaka, T. N. Murakami and H. J. Snaith, *Science*, 2012, **338**, 643.
- J.-H. Im, I.-H. Jang, N. Pellet, M. Grätzel and N.-G. Park, *Nat. Nanotechnol.*, 2014, **9**, 927.
- J. H. Heo, S. H. Im, J. H. Noh, T. N. Mandal, C.-S. Lim, J. A. Chang, Y. H. Lee, H.-j. Kim, A. Sarkar, M. K. Nazeeruddin, M. Grätzel and S. I. Seok, *Nat. Photonics*, 2013, **7**, 486.
- Y. Zhao and K. Zhu, *J. Phys. Chem. Lett.*, 2014, **5**, 4175.
- T. Salim, S. Sun, Y. Abe, A. Krishna, A. C. Grimsdale and Y. M. Lam, *J. Mater. Chem. A*, 2015, DOI: 10.1039/c4ta05226a.
- G. Li, K. L. Ching, J. Y. L. Ho, M. Wong and H.-S. Kwok, *Adv. Energy Mater.*, 2015, 1401775.
- A. Dualeh, N. Tétreault, T. Moehl, P. Gao, M. K. Nazeeruddin and M. Grätzel, *Adv. Funct. Mater.*, 2014, **24**, 3250.
- G. E. Eperon, S. D. Stranks, C. Menelaou, M. B. Johnston, L. M. Herz and H. J. Snaith, *Energy Environ. Sci.*, 2014, **7**, 982.
- Y. Zhao and K. Zhu, *J. Am. Chem. Soc.*, 2014, **136**, 12241.
- P.-W. Liang, C.-Y. Liao, C.-C. Chueh, F. Zuo, S. T. Williams, X.-K. Xin, J. Lin and A. K.-Y. Jen, *Adv. Mater.*, 2014, **26**, 3748.
- Y. Zhao and K. Zhu, *J. Phys. Chem. C*, 2014, **118**, 9412.
- M. I. Dar, N. Arora, P. Gao, S. Ahmad, M. Grätzel and M. K. Nazeeruddin, *Nano Lett.*, 2014, **14**, 6991.
- H. Yu, F. Wang, F. Xie, W. Li, J. Chen and N. Zhao, *Adv. Funct. Mater.*, 2014, **24**, 7102.
- Y. Chen, Y. Zhao and Z. Liang, *Chem. Mater.*, 2015, **27**, 1448.
- S. Colella, E. Mosconi, P. Fedeli, A. Listorti, F. Gazza, F. Orlandi, P. Ferro, T. Besagni, A. Rizzo, G. Calestani, G. Gigli, F. D. Angelis and R. Mosca, *Chem. Mater.*, 2013, **25**, 4613.
- D. Liu, M. K. Gangishetty and T. L. Kelly, *J. Mater. Chem. A*, 2014, **2**, 19873.
- F. Hao, C. C. Stoumpos, Z. Liu, R. P. H. Chang and M. G. Kanatzidis, *J. Am. Chem. Soc.*, 2014, **136**, 16411.
- C. Bi, Y. Shao, Y. Yuan, Z. Xiao, C. Wang, Y. Gao and J. Huang, *J. Mater. Chem. A*, 2014, **2**, 18508.
- D. Shi, V. Adinolfi, R. Comin, M. Yuan, E. Alarousu, A. Buin, Y. Chen, S. Hoogland, A. Rothenberger, K. Katsiev, Y. Losovyj, X. Zhang, P. A. Dowben, O. F. Mohammed, E. H. Sargent and O. M. Bakr, *Science*, 2015, **347**, 519.
- H.-S. Kim, I. Mora-Sero, V. Gonzalez-Pedro, F. Fabregat-Santiago, E. J. Juarez-Perez, N.-G. Park and J. Bisquert, *Nat. Commun.*, 2013, **4**, 2242.
- E. L. Unger, E. T. Hokea, C. D. Bailie, W. H. Nguyen, A. R. Bowringa, T. Heumüller, M. G. Christoforo and M. D. McGehee, *Energy Environ. Sci.*, 2014, **7**, 3690.